Journal of Structural Geology 83 (2016) 180–193

Contents lists available at ScienceDirect

Journal of Structural Geology

journal homepage: www.elsevier.com/locate/jsg

Fabric controls on strain accommodation in naturally deformed mylonites: The influence of interconnected micaceous layers

Nicholas J.R. Hunter [a, *], Pavlína Hasalová [a, b], Roberto F. Weinberg [a], Christopher J.L. Wilson [a]

[a] School of Earth, Atmosphere and Environment, Monash University, Clayton, Victoria, 3800, Australia
[b] Centre for Lithospheric Research, Czech Geological Survey, Klárov 3, Prague 1, 118 21, Czech Republic

ARTICLE INFO

Article history:
Received 16 June 2015
Received in revised form
14 December 2015
Accepted 29 December 2015
Available online 31 December 2015

Keywords:
Main Central Thrust
Zanskar shear zone
Strain partitioning
Second phase
Strain localisation
Crystallographic preferred orientation
Mylonite

ABSTRACT

We present microstructural analyses demonstrating how the geometrical distribution and interconnectivity of mica influences quartz crystallographic preferred orientation (CPO) development in naturally deformed rocks. We use a polymineralic (Qtz + Pl + Kfs + Bt + Ms ± Grt ± Tur) mylonite from the Zanskar Shear Zone, a section of the South Tibetan Detachment (NW Himalaya), to demonstrate how quartz CPO intensity decreases from quartz-dominated domains to micaceous domains, independently of whether or not quartz grains are pinned by mica grains. We then use a bimineralic (Qtz + Ms) mylonite from the Main Central Thrust (NW Himalaya) to show how increasing mica grain connectivity is concomitant with a systematic weakening of quartz CPO. Our results draw distinctions between CPO weakening due to: (i) second phase drag, leading to ineffective recovery in quartz; and (ii) increased transmission and localisation of strain between interconnected mica grains. In the latter case, well-connected micaceous layers take up most of the strain, weakening the rock and preventing straining of the stronger quartz matrix. Our findings suggest that rock weakening in quartz-rich crustal rocks is influenced not only by the presence of mica-rich layers but also the degree of mica grain connectivity, which allows for more effective strain localization through the entire rock mass.

1. Introduction

Identifying strain distribution in lithospheric shear zones depends on our ability to quantify microstructural modifications such as dynamic recrystallization, foliation development, mineral reactions and the formation of crystallographic preferred orientations (CPO; White, 1976; Lister, 1977; Poirier, 1980; Schmid and Casey, 1986; Wenk and Christie, 1991; Hirth and Tullis, 1992; Hippertt and Hongn, 1998; Stipp et al., 2002; Halfpenny et al., 2006; Menegon et al., 2008; Oliot et al., 2010). Microstructures in deformed rocks hold information that can be related to critical physical parameters such as stress, strain rate and temperature, and can be used to derive meaningful kinematic strain paths (Twiss, 1977; Etheridge and Wilkie, 1979; Lister and Hobbs, 1980; Kruhl, 1996; Stipp and Tullis, 2003). However, as continental lithosphere mainly comprises polymineralic rocks with minerals of differing material strengths, the nature of strain distribution, and the rheological behaviour of the lithosphere during deformation, remains poorly understood (Handy, 1990; Ji and Zhao, 1993; Kanagawa et al., 2008; Kilian et al., 2011; Oliot et al., 2014).

It is generally accepted that the bulk rheology of a deforming polymineralic rock is controlled by the weakest phase (Handy, 1990; Schmid and Handy, 1991). In quartzo-feldspathic rocks, abundant and interconnected quartz typically comprises the weak phase and the bulk strength of such rocks is therefore determined by analysing quartz microstructures (Lister and Williams, 1979; Lister and Hobbs, 1980; Fliervoet et al., 1997; Hippertt and Hongn, 1998; Menegon et al., 2008; Mamtani, 2010; Okudaira and Shigematsu, 2012). The assumption that quartz acts as the weakest phase also extends to geodynamic modeling, where crustal strength is typically predicted using quartz dislocation creep laws (Gueydan et al., 2004; Regenauer-Lieb et al., 2006; Regenauer-Lieb and Yuen, 2006; Platt and Behr, 2011). However, changes in rock strength during shear zone evolution cannot be fully understood without an appreciation of the rheological variation arising from strain partitioning into well-developed layers that may contain

* Corresponding author.
E-mail address: nicholas.hunter@monash.edu (N.J.R. Hunter).

http://dx.doi.org/10.1016/j.jsg.2015.12.005
0191-8141/

phases weaker than quartz (Handy, 1990; Holyoke and Tullis, 2006; Gonçalves et al., 2015). Phyllosilicate phases are generally considered to be weaker than quartz and biotite is generally observed to deform more easily than muscovite (Bell and Wilson, 1981). Such phases typically have highly non-linear flow rheologies, low frictional coefficients, and require only minor increases in differential stress, temperature and strain rate in order for crystal plastic deformation to initiate (Etheridge et al., 1973; Shea and Kronenberg, 1993; Mariani et al., 2006).

Most microstructural studies to date have focused on understanding how the volume and dispersion of phyllosilicate phases affect the deformation of a quartz matrix in experimentally sheared aggregates (Wilson, 1979; Olgaard and Evans, 1988; Olgaard, 1990; Tullis and Wenk, 1994; Joy and Saha, 1998) and naturally deformed rocks (Ebert et al., 2007; Song and Ree, 2007; Brodhag et al., 2011). In these studies, the quartz matrix is typically referred to as the 'primary phase' and phyllosilicate phases as the 'second phase'. Conversely, little is known about how the connectivity of these second phases affects quartz deformation (Holyoke and Tullis, 2006; Menegon et al., 2008). Previous studies suggest that, where second phases are highly connected, the stronger quartzofeldspathic matrix will undergo semi-brittle flow and microcracking (Shea and Kronenberg, 1993; Holyoke and Tullis, 2006). A further understanding of how strain is partitioned between micaceous layers and a quartz-dominant matrix may be the basis for understanding rheological changes in naturally deformed polymineralic rocks. Moreover, such investigations are integral in explaining how well-layered polymineralic lithologies, such as schists, accommodate strain during regional shearing; and understanding the role of layering in lithospheric-scale deformation (Montési, 2013).

A principal objective of the current study is to assess the degree to which strain is partitioned between a quartz matrix and variably interconnected micaceous layers. To do this, we have analysed the CPO of the surrounding quartz matrix, in order to understand its response to various degrees of mica fabric development. Under plastic deformation conditions, quartz typically develops a CPO texture, formed due to crystallographic slip along planes at favourable orientations to the critically resolved shear stress (Schmid and Casey, 1986; Heilbronner and Tullis, 2006; Pennacchioni et al., 2010; Muto et al., 2011). The specific slip planes and directions, or 'slip systems', are activated as a function of strain geometry (Schmid and Casey, 1986), temperature (Kruhl, 1996), strain intensity (Lister and Hobbs, 1980), and the presence of fluids (Blacic, 1975). In particular, it is generally agreed that the elevation of shear strains results in stronger CPO maxima (Lister and Hobbs, 1980; Barnhoorn et al., 2004; Heilbronner and Tullis, 2006; Muto et al., 2011). Thus, provided that the quartz is undergoing crystal plastic deformation, the 'strength' of CPO textures provides a valuable means to measure variations in strain accommodation across a sample.

Previous workers have shown that with increasing volume fractions of mica, the CPO of the surrounding quartz matrix becomes increasingly weaker (Olgaard and Evans, 1988; Song and Ree, 2007). It is generally accepted that this is related to the drag forces exerted by mica grains, which inhibit grain growth and dynamic recovery processes in quartz, and subsequently reduce the efficiency of dislocation creep and CPO development (Olgaard, 1990; Herwegh and Berger, 2004; Song and Ree, 2007). Therefore, to fulfil the objectives of our study, a distinction must be drawn between weak CPO development due to: (i) drag forces; and (ii) strain being more effectively accommodated in well-developed, interconnected micaceous layers. Modern facilities, such as the G50 Fabric Analyser, are able to measure and catalogue individual grain orientations, and provide a valuable opportunity to analyze such complexities at the grain scale (Wilson et al., 2007; Peternell et al., 2010). Thus, a methodology that assists in differentiating between these phenomena can be easily developed. A quantitative grain-scale analysis of this type will complement recent observations from deformation experiments (Holyoke and Tullis, 2006), and further strengthen arguments regarding the influence of interconnected micaceous layers on the bulk rheology (Shea and Kronenberg, 1993; Tullis and Wenk, 1994).

In this study, we have investigated deformation fabrics in two samples containing variably connected micaceous layers: (i) a polymineralic orthogneiss mylonite; and (ii) a bimineralic quartz-mica mylonite. We begin by analysing differences at the fabric scale in our orthogneiss mylonite, by comparing quartz CPOs in quartz-rich and mica-rich domains. We then show complexities at the grain scale in our bimineralic mylonite by relating the connectivity of individual mica grains to the CPO of the surrounding quartz matrix, with particular emphasis on the relationship between quartz–quartz, quartz-mica, and mica–mica boundaries. We finish by discussing the implications for interconnected weak layers at the microscopic and regional scale.

2. Sample description

Our polymineralic rock specimen is a highly deformed orthogneiss of the High Himalayan Crystalline sequence exposed at the Zanskar Shear Zone (ZSZ) in the NW Indian Himalaya (Fig. 1; red line). The ZSZ represents the higher end of the South Tibetan Detachment Zone, one of several orogen-parallel ductile shear zones associated with the Himalayan Orogeny (Herren, 1987). Here, top-to-the-SW thrusting is overprinted by an intense top-to-the-NE normal shearing event; the high temperature deformation associated with these events is variably recorded in microstructures of the Higher Himalayan Crystalline rocks (Finch et al., 2014). At the ZSZ boundaries, rocks exhibit clear overprinting relationships between earlier thrust structures and normal shear structures (Finch et al., 2014). Our sample is taken from the shear zone core, where only normal shearing is recorded (Fig. 1; Domain 2a in Finch et al., 2014).

Our bimineralic rock specimen is a quartz-mica mylonite (Qtz – ~85%; Ms – ~15%) collected from the Main Central Thrust (MCT), exposed at the margin of the Kulu-Rampur window in Himachal Pradesh (NW India; Fig. 1; blue line). Here, there is a contact between a 1 km thick Ms-quartz mylonite layer and a Chl-schist layer (32.0106 N 77.24581E; for detailed information on the structure and geology of the Himachal Himalaya, see Bhargava and Bassi, 1994). The thrust at the sample locality strikes 056/27 NW with a strong lineation plunging gently towards the north-east (032–038/16-21). Previous microstructural studies suggest these lithologies were subjected to lower greenschist facies metamorphism (Pandey et al., 2004). Quartzite in this area contains variably stretched and connected muscovite layers, providing a valuable opportunity for understanding the effects of micaceous layers on quartz deformation. Moreover, the simple composition of this rock (one primary matrix phase and one second phase) minimizes the complexity associated with polymineralic rocks.

3. Methods

3.1. Polymineralic mylonite (ZSZ)

In order to measure variations in quartz CPO, we selected three compositional domains within a single thin section sample: (i) a quartz-rich domain (Qtz – 98%; Bt – 2%); (ii) a muscovite-rich domain (Qtz – 77%; Ms – 14%; Bt – 9%); and (iii) a biotite-rich domain (Qtz – 74%; Ms – 2%; Bt – 23%). The use of a single sample ensured that variations in extrinsic factors such as stress, strain

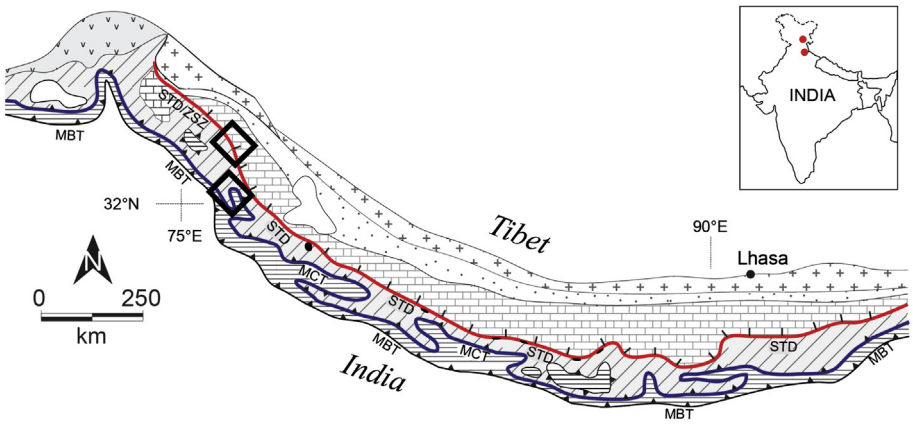

Fig. 1. Simplified map of the Himalaya. Our polymineralic sample is taken from the Zanskar Shear Zone (ZSZ), the upper section of the South Tibetan Detachment Zone (STDZ; red line); our bimineralic sample is taken from the Main Central Thrust (blue line). Squares indicate the location of samples. Inset shows position of sample sites with respect to India. Map adapted from Finch et al. (2014). (For interpretation of the references to colour in this figure legend, the reader is referred to the web version of this article.)

rate and temperature were minimized. CPO data from each domain were collected using a G50 Fabric Analyser at Monash University, and projected onto equal area lower hemisphere pole figures. In addition to collecting bulk CPO datasets from each domain, quartz grains were further divided into subsets based on the number of contacts between quartz and mica grains. Quartz grains not in contact with mica grains are categorized as 'zero order' grains; those in contact with one mica grain are referred to as 'first order' grains; and those in contact with two or more mica grains are referred to as 'second order' grains. The quality of CPO data acquired from the Fabric Analyser is expressed as (i) the geometric quality, which describes the tightness of the intersecting light planes; and (ii) the retardation quality, which describes how well the phase colours of the vertical monochromatic lights match the theoretical interference curves of the Newton colour spectrum (for a detailed description of Fabric Analyser functionality see Peternell et al., 2010). Any data points with geometric and retardation qualities <75 were removed from our data sets, following Peternell et al. (2010). Contouring was calculated using a modified Kamb method (see Vollmer, 1995), with a grid resolution of 30. CPO strength was measured using the eigenvalues of the orientation tensor in each domain, where λ_1 defines the mean eigenvector of the distribution; λ_3 defines the mean eigenvector about the lowest distribution; and λ_2 is the eigenvector perpendicular to λ_1 and λ_3 (Scheidegger, 1965; Woodcock, 1977). The eigenvalues (τ) define the relative magnitude of these eigenvectors, and are normalized (S) so that $S_1 + S_2 + S_3 = 1$. Based on this method, CPO strength has been presented in two ways: (i) ternary diagrams, where the three end members represent point cluster (P), planar girdle (G) or random (R) distributions (Vollmer, 1990); (ii) $1 - R$ values, a measure of non-random c-axis distribution, where 0 represents the complete absence of a CPO.

3.2. Bimineralic rock

We chose several fabric domains based on varying mica contents, and classified these using a number of quantitative measures. Fabric domains were manually digitized using *ArcGIS v10.0*. To ensure a sound statistical representation, a minimum of 300 grains were digitized in each domain. Five fabric domains were analysed using the *MTEX* (https://mtex-toolbox.github.io/) and *PolyLX* (http://petrol.natur.cuni.cz/~ondro/polylx:home) toolboxes in *MATLAB* to quantify the following statistical parameters: (i) volume fraction; (ii) grain size; (iii) aspect ratio; (iv) roundness; (v) lobateness (PARIS factor; Heilbronner and Tullis, 2002); (vi) long axis orientation; and (vii) interparticle distances. CPO data was collected from each fabric domain following the specifications detailed in the previous sub-section.

In order to describe simple relationships between the primary (quartz) and second (muscovite) phases, we applied several additional fabric parameters to our microstructural data (Fig. 2). The ratio between the grain size and volume fraction of the second phase, referred to as the Zener parameter (Z), describes the nature of second phases within a polymineralic medium, where low Z values describe rocks with a large volume fraction of second phase grains and decreased mean interparticle distances between them, and high Z values describe rocks where second phase grains are fewer and more scattered (Herwegh and Berger, 2004). We also use the dispersion factor K to describe the dispersion of the second phase, based on the ratio of the mean interparticle distance between second phase grains and the nearest grain defining the matrix (i.e. quartz), where $K < 1$ describes a matrix with higher second phase interparticle spacing and $K > 1$ describes a matrix with lower second phase interparticle spacing where 'pinning' is more likely (Fig. 2; Brodhag and Herwegh, 2010; Brodhag et al., 2011; Herwegh et al., 2011). Finally, the contact frequencies

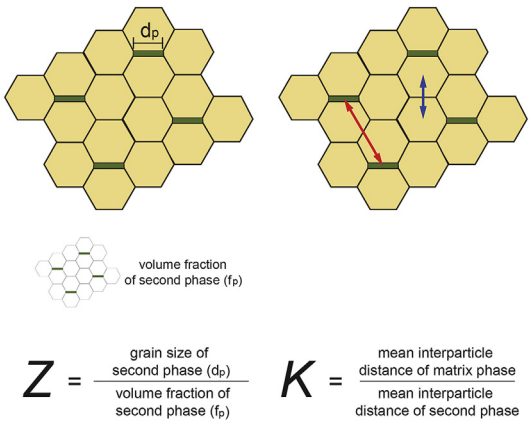

Fig. 2. (A) Schematic representation of the Zener parameter (Z) and dispersion factor (K), defined in Herwegh et al. (2011) and Brodhag et al. (2011). Z is defined as the ratio between the grain size and volume fraction of the second phase. K is defined as the ratio between the mean interparticle distances of matrix grains (blue arrows) and the second phases (red arrows). (For interpretation of the references to colour in this figure legend, the reader is referred to the web version of this article.)

between same phases are expressed in the form of connectivity (*C*). The bulk connectivity of a given phase is defined as the sum of *k*-order connectivity ratios (Eq. (1)):

$$C_k = \sum \frac{b_k}{(b_0 + b_c)} \quad (1)$$

where b_k is the number of connected grains with degree k, b_c is the number of adjacent grains, and b_0 is the number of isolated grains (see Zhanga et al., 1992). Thus, a matrix with no connected grains ($b_k = 0$) will result in a bulk connectivity of zero.

4. Polymineralic mylonite, Zanskar shear zone

4.1. Microstructures

In thin sections cut parallel to the stretching lineation (*XZ* plane), our polymineralic sample comprises Qtz + Pl + Kfs + Bt + Ms ± Grt ± Tur with alternating mica-rich, quartz-rich and feldspar-rich layer-parallel domains (Fig. 3). The primary foliation is well defined across the sample by micaceous layers, which have been sheared to form strong *S*–*C* and *C*' fabrics. There is no evidence of folding or boudinage across the domains, which suggest an equiviscous flow in the specimen (Herwegh and Berger, 2004).

Quartz in the matrix has been dynamically recrystallised and appears as either coarser grains with sutured grain boundaries or as smaller equant grains, which suggests that quartz recrystallization involved both grain boundary migration and sub grain rotation, respectively (Fig. 3B; Hirth and Tullis, 1992). Finch et al. (2014) suggested that the combined activity of these recrystallization mechanisms indicates a deformation temperature range between 490 and 530 °C. The median grain size (Feret diameter) in quartz-rich domains is 93.1 ± 2.5 μm, however coarse grains up to 350 μm are also common (Fig. 4). In mica-rich domains, quartz grain size is less variable, with a median diameter of 60.0 ± 0.9 μm in muscovite-rich domains, and 69.8 ± 1.6 μm in biotite-rich domains (Fig. 4). In these domains, pinning and dragging microstructures are common where quartz is in contact with mica grains (Fig. 3D). K-feldspar and plagioclase porphyroclasts have been deformed in brittle and ductile conditions during the same deformation, as indicated by fracturing in combination with ductile features. Fractures are filled with small recrystallized grains of K-feldspar, plagioclase and quartz. Feldspars are locally flattened, show undulatory extinction and kink bands are common in plagioclase, all suggesting ductile deformation (Yund and Tullis, 1984; Tullis and Yund, 1985, 1987; Finch et al., 2014).

4.2. Crystallographic preferred orientation

Bulk quartz CPO pole figures in Domain 1 (Qtz-rich; Fig. 5) suggest dominant slip along the rhomb-<*a*> and prism-<*a*> glide planes, forming 'single girdle' maxima (Schmid and Casey, 1986). In Domain 2 (muscovite-rich) and Domain 3 (biotite-rich) this maxima is substantially weaker, and there are no discernible differences between zero, first and second order quartz grain subsets. Our *PGR* ternary diagram reveals clear distinctions in the CPO strengths of each domain: Domain 1 exhibits a *G*-dominant distribution, whereas Domains 2 and 3 exhibit *R*-dominant distributions of similar value (Fig. 5C). There are only minor variations in CPO strength amongst the grain subsets; zero order quartz grains (i.e. not in immediate contact with mica grains) show equally weak CPO

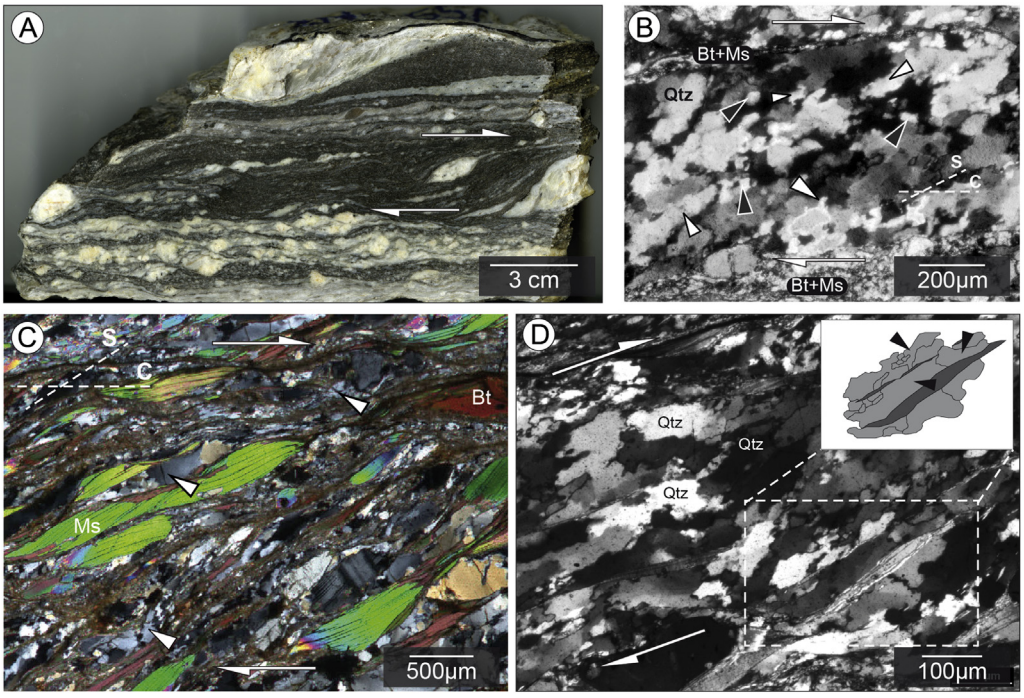

Fig. 3. Characteristic microstructures in the orthogneiss mylonite from the Zanskar Shear Zone, NW Indian Himalaya. (A) Hand specimen cut parallel to the lineation (*XZ* plane). The sample exhibits distinct compositional domains, and shearing is indicated by the orientation of *S* and *C* planes (white arrows). (B) Microstructures inside a typical quartz rich domain, showing dynamically recrystallised quartz grains with shearing indicated by surrounding mica fabrics and shape preferred orientation of quartz grains. Quartz grains are present as larger grains with sutured boundaries (white arrows) or as smaller elliptical grains (grey arrows). An *S*–*C* fabric is defined by quartz shape preferred orientations and mica (Bt + Ms) layers. (C) Microstructures inside a typical mica rich domain, showing detail of *S*–*C* fabrics and quartz rich zones between the layers (white arrows). (D) Quartz grains inside a mica-rich domain, showing evidence of pinning and dragging by muscovite grains. Inset shows detail of pinning (quartz - light grey; muscovite - dark grey).

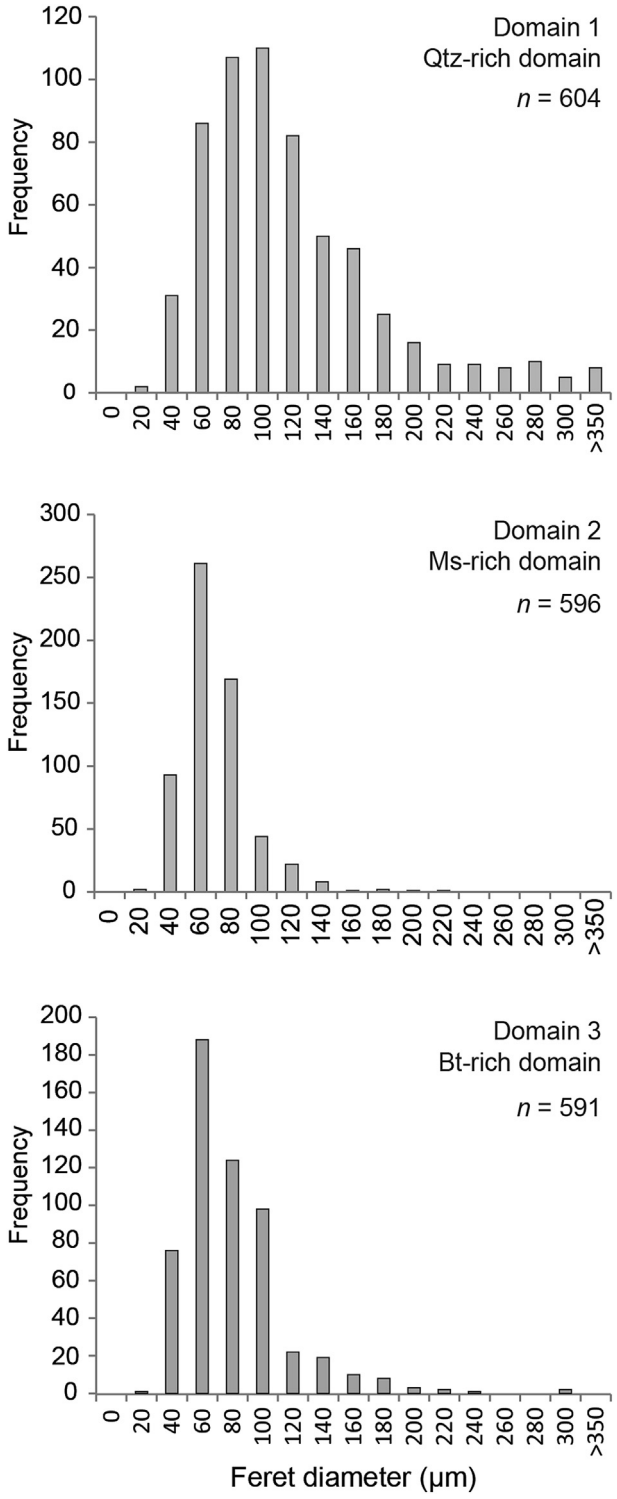

Fig. 4. Grain size distribution histograms for representative quartz-rich, muscovite-rich and biotite-rich domains of the ZSZ mylonite. The number of grains sampled is denoted by *n*.

pole figures as first and second order quartz grains (Fig. 5C).

Overall, there are clear differences in quartz CPO between fabric domains bearing abundant and interconnected quartz, and domains bearing highly connected mica. CPO strength is substantially weakened in the presence of interconnected mica, even in quartz grains not pinned by surrounding mica grains. There appears to be no discernible differences in CPO strength between muscovite-rich and biotite-rich domains.

5. Bimineralic mylonite, Main Central Thrust, Himachal Pradesh

5.1. Microstructures

In thin section, foliations are defined primarily by the orientation of muscovite, which ranges from isolated fine-grained flakes with no significant evidence for shearing (Fig. 6B) to well-developed interconnected bands with *S*–*C* fabrics (Fig. 6C). All domains are layer-parallel, and there is no evidence for folding or boudinage microstructures across the sample, suggesting that the sample deformed under equiviscous conditions (Herwegh and Berger, 2004; Herwegh et al., 2011).

Quartz grains are generally equigranular and exhibit straight extinction, suggesting they are strain free, recrystallised grains formed during dynamic recovery (Fig. 6B–C). Where micaceous layers are present, quartz grains are finer and show evidence of pinning and dragging due to adjacent second phases (Fig. 6C). The polygonal nature of quartz–quartz boundaries suggests that a period of annealing took place, possibly related to a period of static recrystallization.

5.2. Quantitative fabric analysis

A quantitative summary of the microstructural characteristics of the quartz matrix and second phases in each domain is presented in Table 1. We have ordered fabric domains from 1 to 5 based on the increased connectivity of muscovite (C_{Ms}; 0.053 → 0.442 towards Domain 5). In addition, there is a gradual 10% increase in the volume fraction of the second phase towards Domain 5, and the interparticle distance between second phase grains also decreases continuously towards Domain 5 (Fig. 7; Table 1). The changes in proportion and geometry of second phase grains are concurrent with a systematic grain size reduction (Feret diameter) in the quartz matrix (86.4 ± 2.5 μm → 61.2 ± 1.8 μm; Fig. 7). Grain size generally remains between 80 and 90 μm in zero order grains, whereas grain sizes decrease systematically towards Domain 5 in first and second order grains (Table 1). Grain shape variation is minor across the domains, however there are systematic increases in lobateness and aspect ratio between zero, first and second order grains (Table 1).

A number of quantitative measures also describe the relationship between muscovite and the quartz matrix. The dispersion factor (*K*) remains consistently less than 1, which suggests that the maximum grain size of the primary phases is not necessarily controlled by second phases (Brodhag and Herwegh, 2010; Brodhag et al., 2011). However, a distinct shift in Zener parameters is observed between Domains 1–2 (Z = 1000–1100) and Domains 3–5 (Z = ~300). Following the conditions set out by Herwegh and Berger (2004), Domains 1–2 can be categorized as 'dynamic recrystallization controlled' microfabrics, where the steady state quartz grain size is controlled by stress, strain rate and temperature; whereas in Domains 3–5 the matrix grain size lies at the boundary between 'dynamic recrystallization controlled' and 'second phase controlled', which suggests the quartz grain size is controlled by both extrinsic factors and second phases (Fig. 8).

Overall, the five fabric domains demonstrate systematic decreases in quartz grain size and a general decrease in Z (Table 1 and Fig. 7). Conversely, we have found systematic increases in the interparticle distances, connectivity, and volume fraction of second phases from Domains 1 to 5. No appreciable variation was found in the shape (aspect ratio, roundness, lobateness) of grains from Domains 1 to 5, however systematic increases occur between zero,

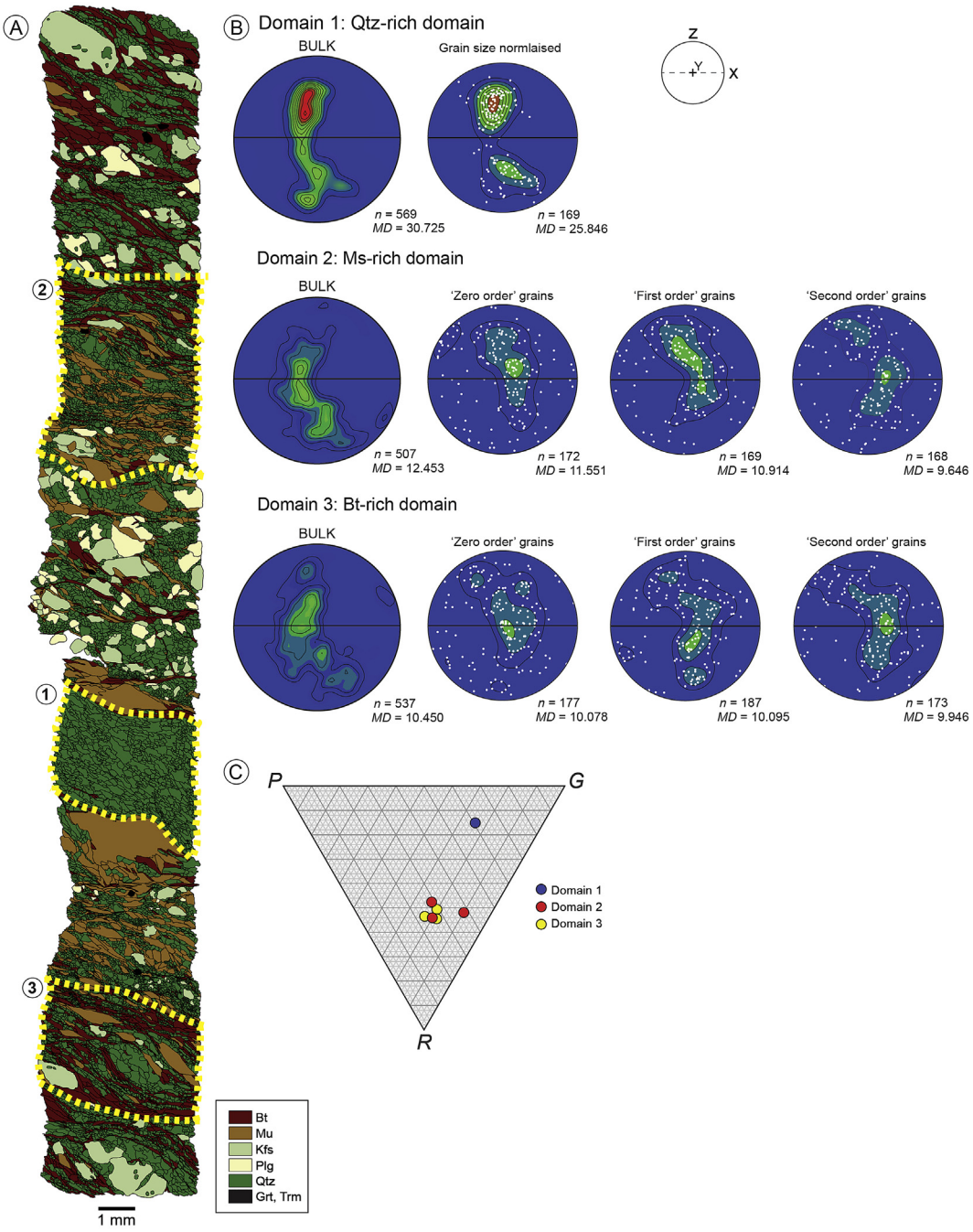

Fig. 5. (A) Digitized grain map for our orthogneiss (polymineralic) mylonite sample, indicating the location of quartz-rich (1), muscovite-rich (2) and biotite-rich (3) compositional domains. (B) *c*-axis [0001] orientation data for quartz with each compositional domain. Data is projected on equal-area lower hemisphere pole figures, contoured at an interval of 2 times the uniform distribution. Pole figures have been rotated so that the foliation is horizontal (black line). n = the number of analysed grains for each projection. *MD* = maximum density of the orientation data. CPO data has been presented for both the bulk rock (left) and for 'zero order', 'first order' and 'second order' grains (refer to text) in each domain. A supplementary pole figure for Domain 1 with a sample size normalised to other grain subsets (n = ~170) is also shown for comparison. (C) *PGR* ternary diagram, indicating the degree to which samples define point (*P*), girdle (*G*), and random (*R*) distributions (Vollmer, 1990).

first and second order grains.

5.3. Crystallographic preferred orientation

In Domains 1 and 2, where muscovite grain connectivity is low (C_{Ms} = 0.053 and 0.070, respectively; Table 1), bulk quartz CPO pole figures suggest well-defined slip along the rhomb-<*a*> glide planes (Fig. 9A; Schmid and Casey, 1986; Heilbronner and Tullis, 2006). The inclination of these maxima is at a low angle to Z, suggesting a simple shearing component (Fig. 9A). Zero, first and second order quartz grains exhibit a similar single girdle structure, however the distributions become more diffuse at second order (note, however, that second order grains are rarer in Domains 1–2; Table 1). In Domains 3, 4 and 5, where muscovite connectivity is high (C_{Ms} = 0.179 – 0.442; Table 1), bulk quartz CPO textures also suggest slip along rhomb-<*a*>, with possible minor slip along basal-<*a*>, but the *c*-axis poles are considerably more scattered (Fig. 9A).

The strength of the bulk quartz CPO becomes weaker from Domain 1 ($1 - R$ = 0.8024) to Domain 5 ($1 - R$ = 0.5824), demonstrating a systematic shift from a *G*-dominant to *R*-dominant

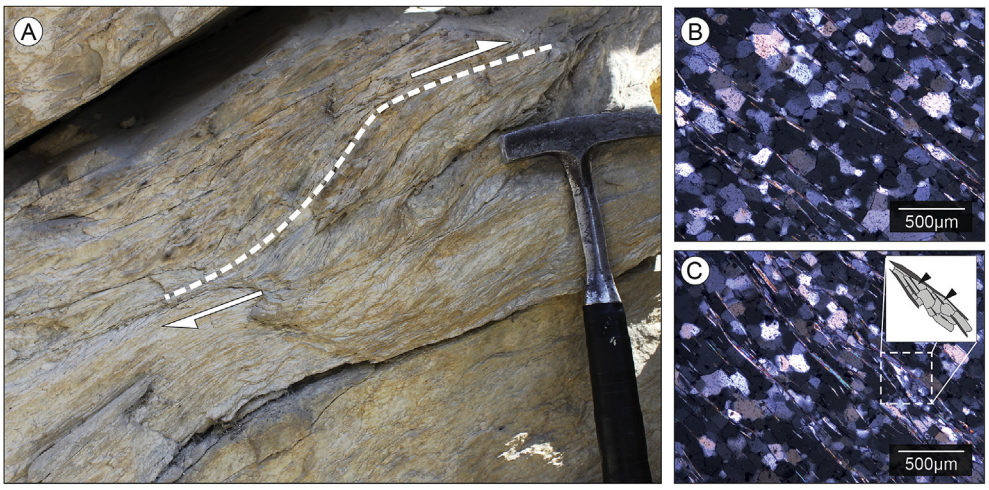

Fig. 6. Field characteristics and microstructures in the quartz-mica (bimineralic) mylonite from the Main Central Thrust (NW Himalaya). (A) Field photo of the sample taken perpendicular to the shear plane. Simple shearing is suggested by strong *S*–*C* fabrics (white arrows). (B) Close-up of a fabric domain where muscovite is fine-grained and poorly connected. Quartz grains are equigranular and show no evidence of pinning or dragging; (C) Close-up of a fabric domain with higher muscovite connectivity. Here, quartz is variably pinned by muscovite (inset, black arrows).

distribution (Fig. 9B). A similar weakening of CPO strength occurs in zero order quartz grains from Domain 1 ($1 - R = 0.8942$) to Domain 4 ($1 - R = 0.6478$), with a similar shift towards an *R*-dominant distribution. While there is a general increase in *R*-dominant distributions in first and second order quartz grains, the variation from Domain 1 to Domain 5 is less systematic. Fig. 10 brings together muscovite connectivity (C_{Ms}) and the bulk CPO strength ($1 - R$) of the quartz matrix in each fabric domain, demonstrating a clear negative correlation between these parameters.

6. Discussion

6.1. Correlations between CPO strength and mica connectivity

The relationship between decreased quartz CPO strength and increased mica connectivity is clear at both the domain scale in our polymineralic sample (Fig. 5), and at the grain scale in our bimineralic sample (Fig. 9). However, the cause of variable CPO strength in quartz still remains unclear, as it could be attributed to four possible processes: (i) drag forces in the second phase (Song and Ree, 2007); (ii) changes in deformation mechanism (Olgaard, 1990); (iii) static annealing (Heilbronner and Tullis, 2002); and (iv) variations in strain accommodation (Lister and Hobbs, 1980). We now discuss these processes separately.

6.1.1. Second phase drag

Increased second phase content typically affects the matrix CPO across a range of rock types (Olgaard and Evans, 1988; Herwegh and Kunze, 2002; Krabbendam et al., 2003; Ebert et al., 2007; Song and Ree, 2007; Linckens et al., 2011; Mamtani and Vishnu, 2012). In many of these studies, samples are shown to have very low *Z* values, indicating that the matrix grain size was controlled by second phases (Herwegh and Berger, 2004; Ebert et al., 2007; Linckens et al., 2011). In the case of quartz-mica fabrics, the volume fraction of second phases only needs an increase of >3% for the quartz CPO to be affected (Song and Ree, 2007). The reasoning behind this inferred relationship between mica content and CPO strength is likely to be that the matrix has a greater exposure to the Zener drag forces associated with mica, leading to a much weaker CPO in the matrix (Ebert et al., 2007; Song and Ree, 2007).

During deformation, anisotropies between neighboring grains can inhibit the effective recovery of grains and result in interparticle strain incompatibility (Means and Jessell, 1986). Ebert et al. (2007) have shown that dislocation densities are higher in calcite grains pinned by second phases than grains that are unpinned. Ebert et al. infer that grain boundary migration, and therefore dislocation movement, was less efficient in the pinned grains. In other words, the rate of dynamic recovery of quartz in areas containing abundant second phases becomes significantly decreased, which is likely to lead to weaker CPOs. There are several lines of evidence in the current study that may suggest the effects of second phase drag in the quartz matrix: (i) pinning and dragging microstructures in each sample (Fig. 3D and Fig. 6C); (ii) weakening of quartz CPO in grains with at least one adjacent mica grain (first and second order grains; Figs. 5 and 9); (iii) decreased grain size in first and second order quartz grains, relative to zero order grains (Table 1); and (iv) where the interparticle distance between second phase grains decreases from Domain 1 to 5 in our bimineralic mylonite (127.9 μm → 73.3 μm; Table 1), there is a corresponding grain size reduction in quartz (86.2 ± 2.5 μm → 61.1 ± 1.8 μm; Table 1).

This provides a partial explanation for weaker CPOs in highly connected mica domains, and also across all first and second order grains (Figs. 5 and 9). However, it does not explain decreased CPO strength in zero order grains. Moreover, it should be noted that *Z* values in our bimineralic sample do not vary considerably from Domain 3 to Domain 5, yet the corresponding *c*-axis distributions of the quartz matrix continue to randomize. In these domains, mica connectivity (C_{Ms}) increases by 26% (Table 1 and Fig. 9). Thus, while we cannot rule out the influence of increased mica saturation on quartz CPO development, it is unlikely that this alone can explain the weak CPOs observed.

6.1.2. Annealing

Some workers have found evidence that static annealing can lead to some minor variations in the strength of a pre-existing CPO, although it is unclear whether this involves CPO weakening (Heilbronner and Tullis, 2002), or CPO strengthening (Augenstein and Burg, 2011). Our bimineralic sample shows evidence of microstructural changes associated with post-deformational annealing (Fig. 6), which raises the possibility that pre-existing CPO textures in this sample may have been subsequently altered, possibly weakened, by later annealing.

There is, however, no evidence to suggest that the various CPOs

Table 1
Representative microstructural analysis of quartz and muscovite grains within different fabric domains of the bimineralic mylonite. Long axis orientation refers to the angle between the long axis of a grain and the shear plane (90°). PARIS factor is a measure of the convexity of a grain (see Heilbronner and Tullis, 2002). Refer to text for explanations of *K* and *Z* parameters.

	Total grains (*N*)				Volume fraction	Grain size (μm)				Aspect ratio				Roundness				PARIS factor (%)				Long axis orientation			
Quartz	**Total**	**Zero**	**First**	**Second**	**Total**	**Total**	**Zero**	**First**	**Second**	**Total**	**Zero**	**First**	**Second**	**Total**	**Zero**	**First**	**Second**	**Total**	**Zero**	**First**	**Second**	**Total**	**Zero**	**First**	**Second**
Domain 1	**256**	96	119	41	**0.9538**	**86.3914**	91.3018	85.8370	80.4614	**1.4323**	1.3988	1.4562	1.5544	**0.5633**	0.5884	0.5642	0.4772	**3.0516**	2.6060	3.0300	4.5622	**11.2383**	22.4412	7.2375	6.6952
Domain 2	**231**	64	99	68	**0.9240**	**76.3659**	83.8688	68.7360	76.3610	**1.5348**	1.5003	1.5279	1.6001	**0.5581**	0.5789	0.5640	0.5410	**1.3508**	0.9774	1.2260	2.9910	**3.6812**	11.2725	0.8261	3.1557
Domain 3	**244**	52	111	79	**0.8787**	**68.8277**	89.6389	65.7310	68.6357	**1.6171**	1.4309	1.6570	1.6872	**0.5379**	0.5730	0.5322	0.5240	**1.9000**	1.5430	1.9011	2.1636	**6.5710**	24.9047	5.6884	3.4620
Domain 4	**253**	45	129	74	**0.8660**	**62.6263**	80.1321	67.2944	61.2478	**1.5791**	1.3117	1.4915	2.0298	**0.5370**	0.6510	0.5700	0.4447	**1.2450**	0.8864	1.3201	1.2450	**1.7651**	9.7458	4.8357	0.0742
Domain 5	**263**	41	93	129	**0.8528**	**61.1980**	91.0635	66.3030	60.4837	**1.7031**	1.5461	1.8444	2.0707	**0.4868**	0.5890	0.5100	0.4830	**2.1120**	1.9473	3.0769	3.5750	**3.6688**	16.7803	3.9640	5.2691
Mica	**Total**				**Total**	**Total**				**Total**				**Total**				**Total**				**Total**			
Domain 1	**57**	–	–	–	**0.046**	**49.655**	–	–	–	**6.396**	–	–	–	**0.142**	–	–	–	**0.142**	–	–	–	**1.560**	–	–	–
Domain 2	**77**	–	–	–	**0.076**	**84.629**	–	–	–	**7.396**	–	–	–	**0.145**	–	–	–	**0.145**	–	–	–	**0.197**	–	–	–
Domain 3	**66**	–	–	–	**0.121**	**40.389**	–	–	–	**8.108**	–	–	–	**0.120**	–	–	–	**0.120**	–	–	–	**0.184**	–	–	–
Domain 4	**61**	–	–	–	**0.134**	**42.451**	–	–	–	**10.679**	–	–	–	**0.086**	–	–	–	**0.086**	–	–	–	**0.251**	–	–	–
Domain 5	**77**	–	–	–	**0.147**	**50.325**	–	–	–	**7.948**	–	–	–	**0.100**	–	–	–	**0.100**	–	–	–	**1.123**	–	–	–

	Interparticle distance (μm)		Connectivity (C_{Ms})	Dispersion factor (*K*)	Zener parameter (*Z*)
	Quartz	Mica			
Domain 1	66.4690	127.9192	0.0526	0.5196	1074.7710
Domain 2	56.9358	86.1598	0.0702	0.6608	1113.7289
Domain 3	51.3535	75.1352	0.1786	0.6835	333.0476
Domain 4	46.5774	74.9788	0.2000	0.6212	316.7147
Domain 5	46.7689	73.2800	0.4416	0.6382	341.9403

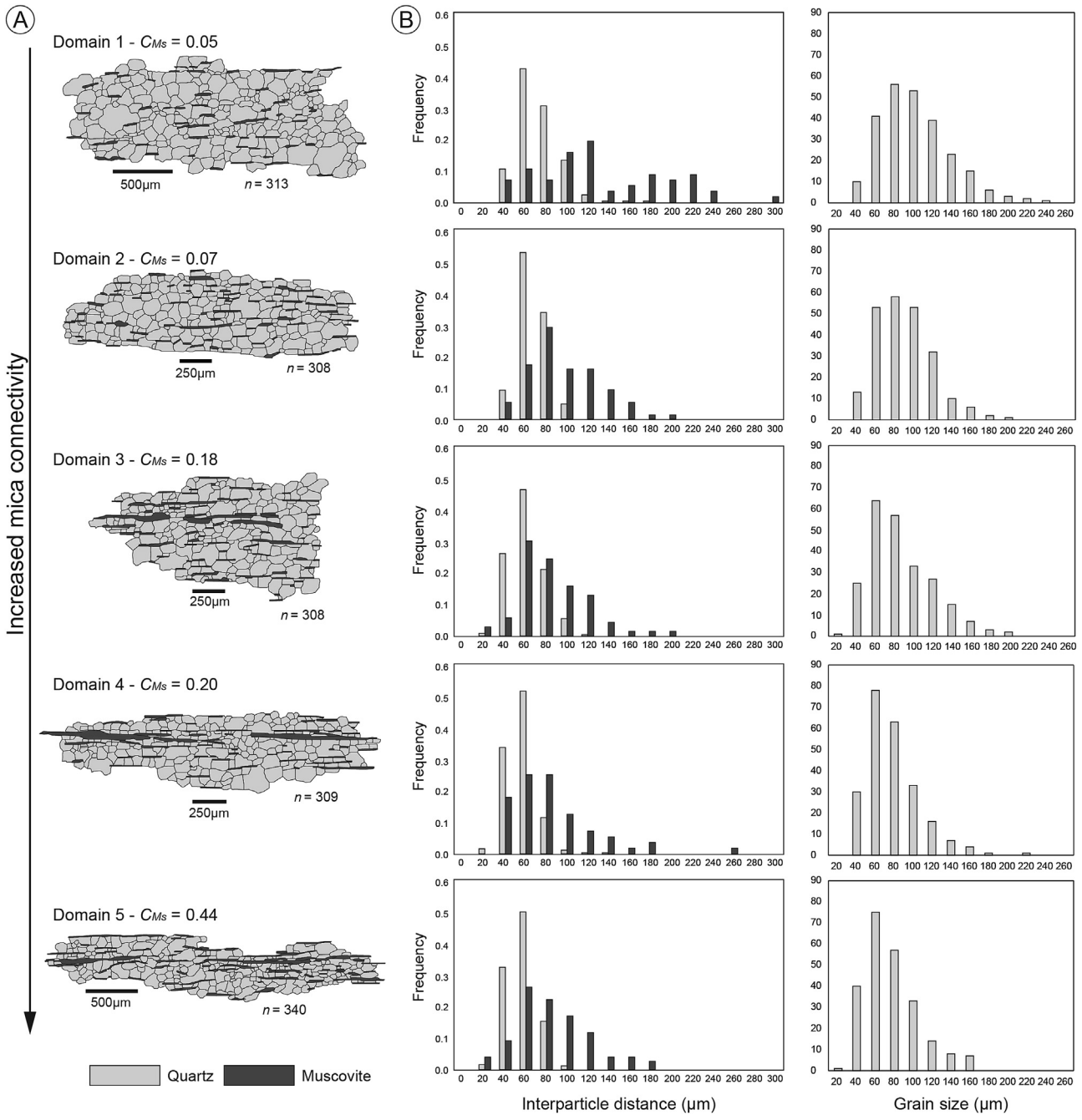

Fig. 7. (A) Digitized images of compositional domains from the bimineralic mylonite, with corresponding connectivity of the second phase (C_{Ms}). n = number of grains digitized; (B) Interparticle spacing between quartz (light grey) and muscovite (dark grey) grains, calculated from the mean vector distance to the nearest neighbour grain. Note the decreased interparticle spacing of the second phase (Ms) towards Domain 5. (C) Grain size distribution histograms (Feret diameter) for quartz grains in each domain.

across the domains were affected. Quartz-rich domains (Domains 1–2) still contain a strong CPO, with no clear evidence of scattering in the *c*-axis distribution (Fig. 9A). More importantly, even if the sample was affected by a period of annealing, it did not erase the relative differences in CPO weakening per domain, which is the critical element in our study. If quartz-rich areas appear to retain their CPO quite effectively, it should follow that zero order grains in other domains should also retain their CPOs. Conversely, there is a systematic weakening in the CPO of these grains (Fig. 9). It should also be pointed out that the possibility of annealing does not explain the CPO weakening processes observed in our polymineralic sample, where annealing is absent. Overall, we argue that, while microstructures might suggest annealing conditions in this sample (Fig. 6), it is unlikely that it contributed to the variably weak CPOs observed.

6.1.3. Local changes in deformation mechanism

Various studies have suggested that microfabrics containing second phases can undergo a localized switch from a grain size insensitive creep (GSI) mechanism (e.g. dislocation creep) to a grain size sensitive mechanism (GSS) (Olgaard, 1990; Krabbendam et al., 2003; Linckens et al., 2011). The main lines of evidence for this

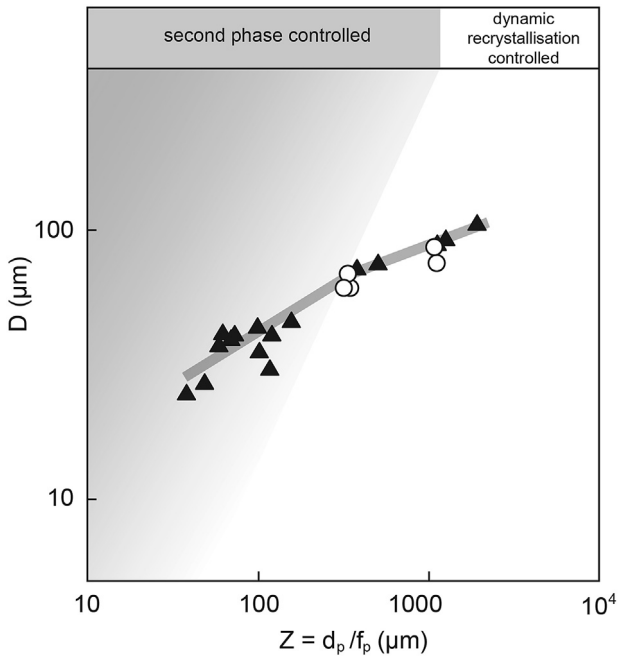

Fig. 8. Zener plot defining the transition from dynamic recrystallization controlled to second phase controlled microstructures as a function of Zener parameter (Z) and quartz grain size (D). Circles are various domains from the sample used in the current study (refer to text). Black triangles are samples from Song and Ree (2007). Modified from Herwegh et al. (2011).

rheological transition is the existence of very diffuse CPOs, as well as the mixing of phases to form a homogeneous, equigranular fabric in polymineralic rocks (Fliervoet et al., 1997; Wightman et al., 2006; Kilian et al., 2011; Linckens et al., 2011).

There are several lines of evidence that suggest this is not the case in our samples. Firstly, the common occurrence of a single girdle CPO in each domain, albeit with variable CPO strength, suggests that GSI creep was an active deformation mechanism in both our study samples (Fig. 9). Secondly, experimental studies suggest that, given the observed grain sizes across our samples (~60–100 μm), the activation of grain size sensitive creep at greenschist-amphibolite conditions is improbable (Brodie and Rutter, 2000; Rutter and Brodie, 2004). In natural settings, evidence for GSS flow in quartz-bearing rocks under these conditions has generally been associated with grain sizes <50 μm (Fliervoet et al., 1997; Song and Ree, 2007; Kilian et al., 2011; Oliot et al., 2014). In quartzites, grain sizes <10 μm are typically required for GSS flow to be activated (Behrmann, 1985; Rutter and Brodie, 2004). It is therefore unlikely that CPO weakening can be explained by a local switch to GSS deformation mechanisms.

6.1.4. Strain localisation in micaceous layers

Our observations thus far suggest that second phase drag provides the only reasonable answer for CPO weakening. However, we have attempted to distinguish between CPO weakening due to drag force factors, and weakening due to strain partitioning into well-connected micaceous layers. A significant observation supporting the latter is the apparent weakening of CPO in quartz grains not in immediate contact with micas (zero order grains), which is relevant to both samples studied (Figs. 5 and 9). In these instances, weak CPOs cannot be explained by Zener drag forces from a second phase and therefore the lack of strain accommodation in these grains may suggest that strain was more easily accommodated in the adjacent micaceous layers. Quartz grains in the matrix of these domains were less strained and likely underwent slower cycles of recrystallization relative to quartz-rich domains, and thus unfavourably oriented grains tended to remain in the sample (Herwegh and Kunze, 2002; Ebert et al., 2007). Combined, the processes of mica pinning and localization into micaceous layers resulted in the quartz CPO being underdeveloped in domains where mica is highly connected.

The localization of strain into highly connected mica layers has been suggested as a process in experimentally deformed quartzites (Tullis and Wenk, 1994) and naturally deformed mylonites (Menegon et al., 2008). Previous workers have also suggested that the high phase strength contrast that develops between increasingly interconnected mica and the quartz matrix results in localized shear zones and subsequent strain weakening in mica (Shea and Kronenberg, 1993; Holyoke and Tullis, 2006). Our study complements these observations by demonstrating the local response of the quartz matrix with increased grain connectivity, in the form of a weak CPO (Figs. 5 and 9).

A final point of consideration is how representative the current data is when considering the grain neighbor relationships in three dimensional space, as one may argue that 'zero order' grains may in fact be pinned by mica grains with their continuation into the third dimension. This would mean that their quantification in a two dimensional section is prone to misrepresentation. While we cannot completely rule this out as a confounding variable, there are several observations in our bimineralic sample that suggest this to be of minor concern. Firstly, our aspect ratio and PARIS factor statistics show systematic increases from zero order to second order grains in each domain, suggesting that variations in grain shape occur as a result of increased contact with mica grains (Table 1). If all grains were equally pinned to some extent in three dimensional space, these grain shape values would be reasonably consistent across the datasets. Secondly, in addition to the clear transitions in CPO weakening from Domain 1 to 5, our ternary diagrams show that there are also distinct differences in the range of CPO intensity values between the various grain orders (zero order grains: $1-R = 0.8942-0.6478$; second order grains: $1-R = 0.7113-0.4494$). In second order grains, it is likely that both drag forces and increased mica connectivity affect the CPO strength, producing a lower range of CPO strength values compared to the zero order grains, which are only subjected to CPO weakening associated with increased mica connectivity. If pinning affected all grains in three dimensional space, it is likely that the range of CPO intensity values across the three orders would be similar. Thus, on the basis of these observations, we argue that consideration of the three dimensional continuation of fabric domains in our samples is not required.

Overall, our results show that CPO development in mylonitic rocks containing an interconnected quartz matrix is controlled not only by the pinning and dragging of second phases but also their connectivity. Where mica interconnectivity is higher, the weak CPO of the surrounding quartz matrix reflects a combination of (i) decreases in the rate of dynamic recovery in quartz grains due to the drag forces exerted by mica; and (ii) the localisation of strain into micaceous layers.

6.2. Implications for regional scale deformation

If one assumes that crustal deformation is scale independent, our observations carry important implications for macro-scale shear zone evolution and the rheology of the crust. In polymineralic rocks undergoing non-linear flow, assuming that the bulk rheology is dependent in part on the connectivity of its weak and strong mineral constituents, the formation of fabrics that align with the shear direction can instigate a rheological switch from a matrix-

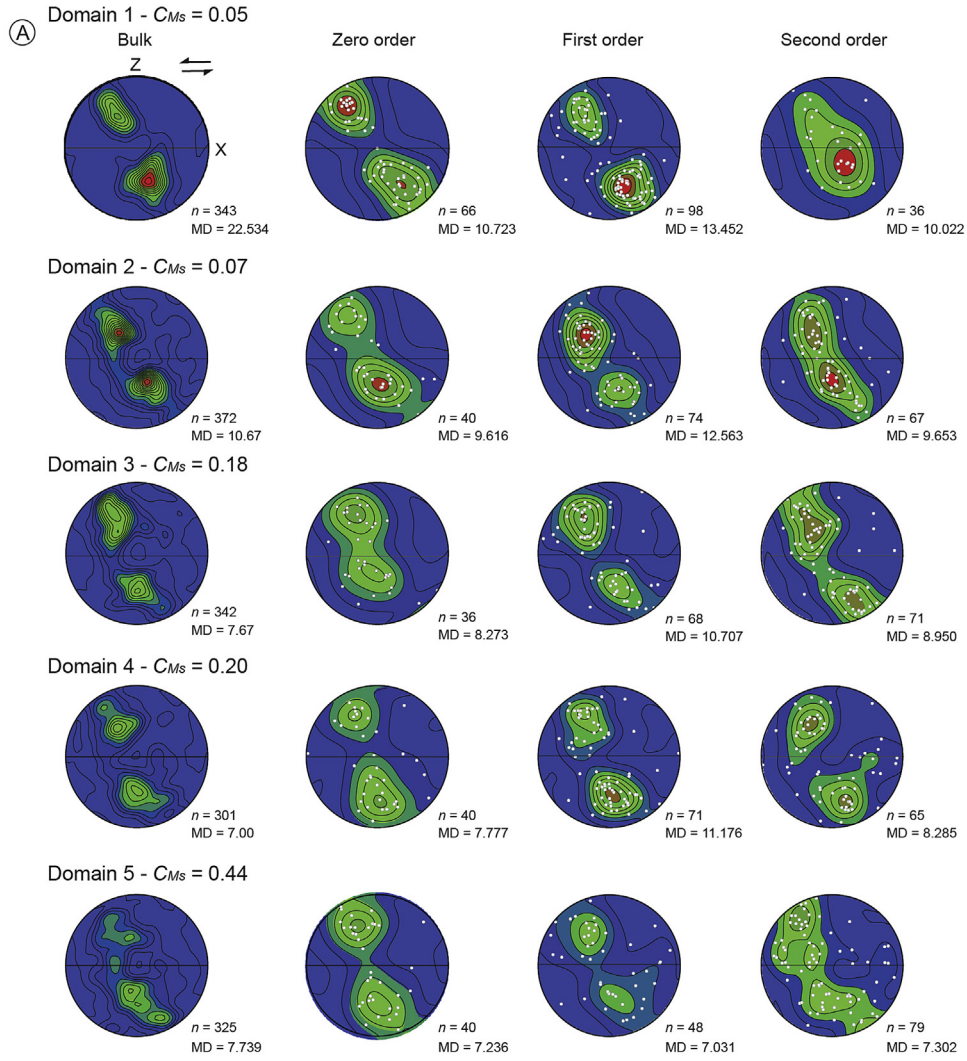
Ⓐ
Domain 1 - C_{MS} = 0.05
Bulk
Zero order
First order
Second order
Z
X
n = 343
MD = 22.534
n = 66
MD = 10.723
n = 98
MD = 13.452
n = 36
MD = 10.022
Domain 2 - C_{MS} = 0.07
n = 372
MD = 10.67
n = 40
MD = 9.616
n = 74
MD = 12.563
n = 67
MD = 9.653
Domain 3 - C_{MS} = 0.18
n = 342
MD = 7.67
n = 36
MD = 8.273
n = 68
MD = 10.707
n = 71
MD = 8.950
Domain 4 - C_{MS} = 0.20
n = 301
MD = 7.00
n = 40
MD = 7.777
n = 71
MD = 11.176
n = 65
MD = 8.285
Domain 5 - C_{MS} = 0.44
n = 325
MD = 7.739
n = 40
MD = 7.236
n = 48
MD = 7.031
n = 79
MD = 7.302

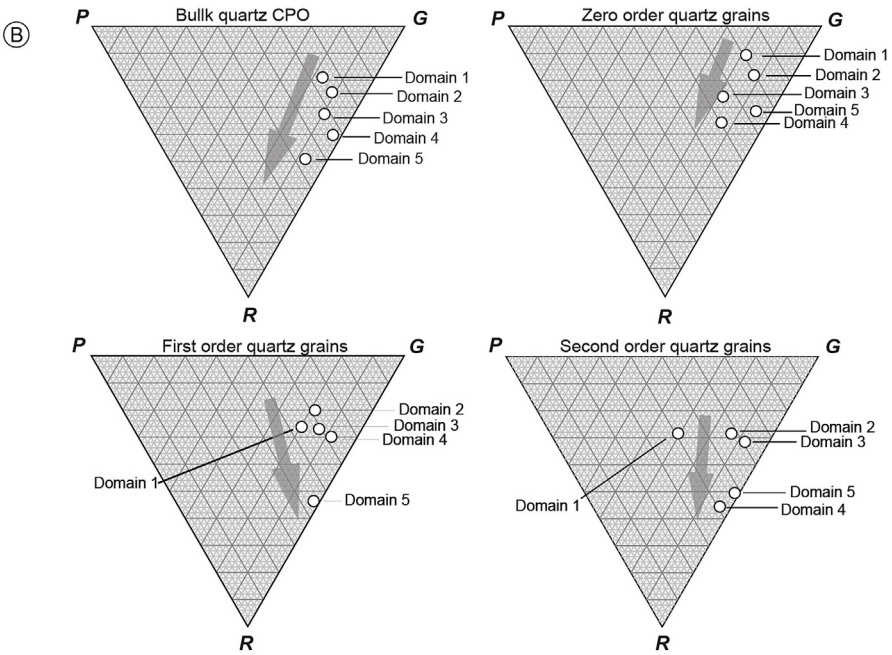
Ⓑ
P
G
R
Bullk quartz CPO
Domain 1
Domain 2
Domain 3
Domain 4
Domain 5
Zero order quartz grains
First order quartz grains
Second order quartz grains

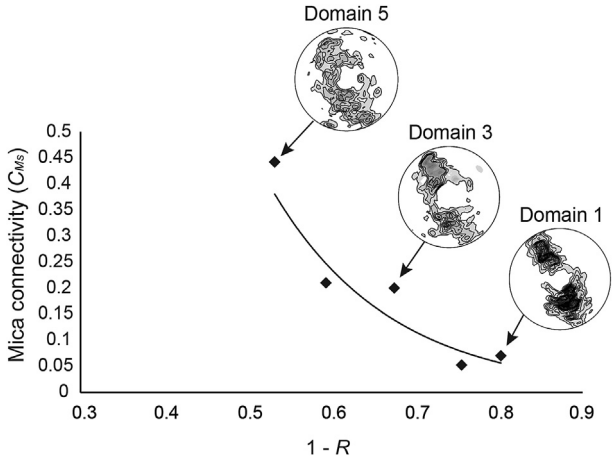

Fig. 10. Mica connectivity (C_{Ms}) versus the CPO intensity in fabric domains of the bimineralic mylonite. 1-*R* is a measure of the degree of non-random distribution in the CPO projection, based on eigenvalues of the orientation data (see Fig. 9).

supported rheology to interconnected weak layer-supported rheology (Handy, 1990). This shift is commonly observed in experimentally deformed rocks (Jordan, 1987; Tullis and Wenk, 1994; Gonçalves et al., 2015). Montési (2013) has used analytical expressions to emphasize the high localization potential of rocks with layered fabrics in a shear zone, which arises due to the major strength anisotropies between the layered fabric and the surrounding wall rock. Given the highly non-linear flow of phyllosilicates (Mariani et al., 2006), it follows that rocks with well-developed micaceous fabrics may localize strain more effectively than matrix supported rocks (Handy, 1990). Several studies have shown how the development of such fabrics resulted in increased ductile shearing at strain rates several orders of magnitude higher than the surrounding rock (Johnson et al., 2004; Park et al., 2006; Rennie et al., 2013). It is less clear how interconnected weak layers play a role in shear zones undergoing linear viscous flow conditions (e.g. diffusion creep), however recent studies by Oliot et al. (2014) suggest that they are integral in localising deformation along shear bands and driving fluid advection.

Our microstructural analyses give further insight into how these interconnected weak layers are reflected at the micro-scale of sialic crustal rocks undergoing ductile deformation: the development of well-connected micaceous layering is intimately related to the degree of deformation taken up by the quartz matrix, even in grains unperturbed by second phase drag. The increased transmission and localization of strain between interconnected mica grains, as observed here, may be particularly important in interlayered gneiss/schist units, where ductile shearing can be effectively localized in schists. Like at microscale, here it is not only the presence of schists that play a role, but the degree to which they are interconnected across the orogeny, that influences strain localization through the rock mass. A major shortcoming in current geological methods is the absence of a robust method for assessing mica deformation in naturally deformed rocks, as well as the absence of a robust flow law (Passchier and Trouw, 2005). Thus, a key requirement for future studies is the development of identifiable crystal defect criteria in phyllosilicates (e.g. Bell and Wilson, 1981), which can be used to evaluate the partitioning of deformation between the primary and second phases of a deforming medium.

7. Conclusions

We applied quantitative microstructural analyses on naturally deformed polymineralic and bimineralic mylonites with variably connected mica fabrics, in order to investigate the impact of mica interconnectivity on CPO development in the surrounding quartz matrix. Quartz CPO in our polymineralic sample reveal distinct strength differences across different fabrics (quartz-rich domain: $1 - R = 0.8490$; muscovite-rich domain: $1 - R = 0.4343$; biotite-rich domain: $1 - R = 0.4492$; Fig. 5). In our bimineralic mylonite, increases in mica connectivity ($C_{Ms} = 0.053 \rightarrow 0.442$) are concomitant with a systematic weakening of quartz CPO ($1 - R = 0.8024 \rightarrow 0.5824$), even where quartz grains are not in contact with mica grains ($1 - R = 0.8942 \rightarrow 0.7428$; Fig. 9). It is likely that the decreased CPO strengths observed were caused by: (i) increased dragging of quartz grains from mica, inhibiting their effective dynamic recovery; and (ii) increased transmission and localisation of strain in layers containing interconnected mica grains (Figs. 5 and 9). Micaceous fabrics may be integral to understanding regional tectonics, where rocks bearing well-connected phyllosilicates, such as schists, accommodate strain more readily than quartz-rich rocks.

Acknowledgements

Pavlina Hasalová acknowledges funding from the Ministry of Education of the Czech Republic (grant LK11202). We thank also Geoffrey Lloyd and the School of Earth And Environment at Leeds University for the use of their facilities; and Mark Peternell of Johannes Gutenberg-Universität Mainz for his detailed discussions on the topic of this paper. Finally, we thank Marco Herwegh and Luca Menegon for their detailed feedback on our original manuscript.

References

Augenstein, C., Burg, J.P., 2011. Natural annealing of dynamically recrystallised quartzite fabrics: example from the Cévennes, SE French Massif Central. J. Struct. Geol. 33, 244–254.
Barnhoorn, A., Bystricky, M., Burlini, L., Kunze, K., 2004. The role of recrystallisation on the deformation behaviour of calcite rocks: large strain torsion experiments on Carrara marble. J. Struct. Geol. 26, 885–903.
Behrmann, J.H., 1985. Crystal plasticity and superplasticity in quartzite; A natural example. Tectonophysics 115, 101–129.
Bell, I.A., Wilson, C.J.L., 1981. Deformation of biotite and muscovite: TEM microstructure and deformation model. Tectonophysics 78, 201–228.
Bhargava, O.N., Bassi, U.K., 1994. The crystalline thrust sheets in the Himachal Himalaya and the age of amphibolite facies metamorphism. Geol. Soc. India 43, 343–352.
Blacic, J.D., 1975. Plastic deformation mechanisms in quartz: the effect of water. Tectonophysics 27, 271–294.
Brodhag, S., Herwegh, M., 2010. The effect of different second-phase particle regimes on grain growth in two-phase aggregates: insights from in situ rock analogue experiments. Contrib. Mineral. Petrol. 160, 219–238.
Brodhag, S.H., Herwegh, M., Berger, A., 2011. Grain coarsening in polymineralic contact metamorphic carbonate rocks: the role of different physical interactions during coarsening. J. Struct. Geol. 33, 698–712.
Brodie, K.H., Rutter, E.H., 2000. Deformation mechanisms and rheology: why marble is weaker than quartzite. J. Geol. Soc. 157, 1093–1096.
Ebert, A., Herwegh, M., Evans, B., Pfiffner, A., Austin, N., Vennemann, T., 2007.

Fig. 9. (A) *c*-axis orientation data for all domains in the bimineralic mylonite, including zero, first, and second order quartz grain subsets (refer to text). Muscovite connectivity is denoted by *C*, after Zhanga et al. (1992), and increases towards Domain 5. *n* = the number of analysed grains for each projection. *MD* = maximum density of the orientation data. Due to their lower sample sizes, CPO data for zero, first and second order quartz grains are presented as both contours and points (white); (B) *PGR* diagrams, based on the eigenvalues of the orientation data across CPO textures, and representing a measure of the degree to which the orientation data define point (*P*), girdle (*G*) or random (*R*) distributions. Note the systematic increase in random distributions with increased mica connectivity in each projection.

Microfabrics in carbonate mylonites along a large-scale shear zone (Helvetic Alps). Tectonophysics 444, 1–26.
Etheridge, M.A., Hobbs, B.E., Paterson, M.S., 1973. Experimental deformation of single crystals of biotite. Contrib. Mineral. Petrol. 38, 21–36.
Etheridge, M.A., Wilkie, J.C., 1979. Grainsize reduction, grain boundary sliding and the flow strength of mylonites. Tectonophysics 58, 159–178.
Finch, M., Hasalová, P., Weinberg, R.F., Fanning, C.M., 2014. Switch from thrusting to normal shearing in the Zanskar shear zone, NW Himalaya: Implications for channel flow. Geol. Soc. Am. Bull. 126, 892–924.
Fliervoet, T.F., White, S.H., Drury, M.R., 1997. Evidence for dominant grain-boundary sliding deformation in greenschist- and amphibolite-grade polymineralic ultramylonites from the redbank deformed Zone, Central Australia. J. Struct. Geol. 19, 1495–1520.
Gonçalves, C.C., Gonçalves, L., Hirth, G., 2015. The effects of quartz recrystallization and reaction on weak phase interconnection, strain localization and evolution of microstructure. J. Struct. Geol. 71, 24–40.
Gueydan, F., Leroy, Y.M., Jolivet, L., 2004. Mechanics of low-angle extensional shear zones at the brittle-ductile transition. J. Geophys. Res. Solid Earth 109, B12407.
Halfpenny, A., Prior, D.J., Wheeler, J., 2006. Analysis of dynamic recrystallization and nucleation in a quartzite mylonite. Tectonophysics 427, 3–14.
Handy, M.R., 1990. The solid-state flow of polymineralic rocks. J. Geophys. Res. 95, 8647–8661.
Heilbronner, R., Tullis, J., 2002. The effect of static annealing on microstructures and crystallographic preferred orientations of quartzites experimentally deformed in axial compression and shear. Geological Society, London. Spec. Publ. 200, 191–218.
Heilbronner, R., Tullis, J., 2006. Evolution of c axis pole figures and grain size during dynamic recrystallization: results from experimentally sheared quartzite. J. Geophys. Res. Solid Earth 111, B10202.
Herren, E., 1987. Zanskar shear zone: northeast-southwest extension within the higher Himalayas (Ladakh, India). Geology 15, 409–413.
Herwegh, M., Berger, A., 2004. Deformation mechanisms in second-phase affected microstructures and their energy balance. J. Struct. Geol. 26, 1483–1498.
Herwegh, M., Kunze, K., 2002. The influence of nano-scale second-phase particles on deformation of fine grained calcite mylonites. J. Struct. Geol. 24, 1463–1478.
Herwegh, M., Linckens, J., Ebert, A., Berger, A., Brodhag, S.H., 2011. The role of second phases for controlling microstructural evolution in polymineralic rocks: a review. J. Struct. Geol. 33, 1728–1750.
Hippertt, J.F., Hongn, F.D., 1998. Deformation mechanisms in the mylonite/ultramylonite transition. J. Struct. Geol. 20, 1435–1448.
Hirth, G., Tullis, J., 1992. Dislocation creep regimes in quartz aggregates. J. Struct. Geol. 14, 145–159.
Holyoke, C.W., Tullis, J., 2006. Mechanisms of weak phase interconnection and the effects of phase strength contrast on fabric development. J. Struct. Geol. 28, 621–640.
Ji, S., Zhao, P., 1993. Flow laws of multiphase rocks calculated from experimental data on the constituent phases. Earth Planet. Sci. Lett. 117, 181–187.
Johnson, S.E., Vernon, R.H., Upton, P., 2004. Foliation development and progressive strain-rate partitioning in the crystallizing carapace of a tonalite pluton: microstructural evidence and numerical modeling. J. Struct. Geol. 26, 1845–1865.
Jordan, P.G., 1987. The deformational behaviour of bimineralic limestone-halite aggregates. Tectonophysics 135, 185–197.
Joy, S., Saha, D., 1998. Influence of micaceous impurity on dynamically recrystallized quartz c-axis fabric in L-S tectonites from the Singhbhum shear zone and its footwall, eastern India. J. Struct. Geol. 20, 1509–1520.
Kanagawa, K., Shimano, H., Hiroi, Y., 2008. Mylonitic deformation of gabbro in the lower crust: a case study from the Pankenushi gabbro in the Hidaka metamorphic belt of central Hokkaido, Japan. J. Struct. Geol. 30, 1150–1166.
Kilian, R., Heilbronner, R., Stünitz, H., 2011. Quartz grain size reduction in a granitoid rock and the transition from dislocation to diffusion creep. J. Struct. Geol. 33, 1265–1284.
Krabbendam, M., Urai, J.L., van Vliet, L.J., 2003. Grain size stabilisation by dispersed graphite in a high-grade quartz mylonite: an example from Naxos (Greece). J. Struct. Geol. 25, 855–866.
Kruhl, J.H., 1996. Prism- and basal-plane parallel subgrain boundaries in quartz: a microstructural geothermobarometer. J. Metamorph. Geol. 14, 581–589.
Linckens, J., Herwegh, M., Müntener, O., Mercolli, I., 2011. Evolution of a polymineralic mantle shear zone and the role of second phases in the localization of deformation. J. Geophys. Res. Solid Earth 116. B06210.
Lister, G.S., 1977. Crossed-girdle c-axis fabrics in quartzites plastically deformed by plane strain and progressive simple shear. Tectonophysics 39, 51–54.
Lister, G.S., Hobbs, B.E., 1980. The simulation of fabric development during plastic deformation and its application to quartzite: the influence of deformation history. J. Struct. Geol. 2, 355–370.
Lister, G.S., Williams, P.F., 1979. Fabric development in shear zones: theoretical controls and observed phenomena. J. Struct. Geol. 1, 283–297.
Mamtani, M., Vishnu, C., 2012. Does AMS data from micaceous quartzite provide information about shape of the strain ellipsoid? Int. J. Earth Sci. 101, 693–703.
Mamtani, M.A., 2010. Strain rate estimation using fractal analysis of quartz grains in naturally deformed rocks. J. Geol. Soc. India 75, 202–209.
Mariani, E., Brodie, K.H., Rutter, E.H., 2006. Experimental deformation of muscovite shear zones at high temperatures under hydrothermal conditions and the strength of phyllosilicate-bearing faults in nature. J. Struct. Geol. 28, 1569–1587.
Means, W.D., Jessell, M.W., 1986. Accommodation migration of grain boundaries. Tectonophysics 127, 67–86.
Menegon, L., Pennacchioni, G., Heilbronner, R., Pittarello, L., 2008. Evolution of quartz microstructure and c-axis crystallographic preferred orientation within ductilely deformed granitoids (Arolla unit, western Alps). J. Struct. Geol. 30, 1332–1347.
Montési, L.G.J., 2013. Fabric development as the key for forming ductile shear zones and enabling plate tectonics. J. Struct. Geol. 50, 254–266.
Muto, J., Hirth, G., Heilbronner, R., Tullis, J., 2011. Plastic anisotropy and fabric evolution in sheared and recrystallized quartz single crystals. J. Geophys. Res. Solid Earth 116. B02206.
Okudaira, T., Shigematsu, N., 2012. Estimates of stress and strain rate in mylonites based on the boundary between the fields of grain-size sensitive and insensitive creep. J. Geophys. Res. B Solid Earth 117.
Olgaard, D.L., 1990. The Role of Second Phase in Localizing Deformation, 54. Special Publications, Geological Society, London, pp. 175–181.
Olgaard, D.L., Evans, B., 1988. Grain growth in synthetic marbles with added mica and water. Contrib. Mineral. Petrol. 100, 246–260.
Oliot, E., Goncalves, P., Marquer, D., 2010. Role of plagioclase and reaction softening in a metagranite shear zone at mid-crustal conditions (Gotthard Massif, Swiss Central Alps). J. Metamorph. Geol. 28, 849–871.
Oliot, E., Goncalves, P., Schulmann, K., Marquer, D., Lexa, O., 2014. Mid-crustal shear zone formation in granitic rocks: constraints from quantitative textural and crystallographic preferred orientations analyses. Tectonophysics 612–613, 63–80.
Pandey, A.K., Sachan, H.K., Virdi, N.S., 2004. Exhumation history of a shear zone constrained by microstructural and fluid inclusion techniques: an example from the Satluj valley, NW Himalaya, Indian. J. Asian Earth Sci. 23, 391–406.
Park, Y., Yoo, S.-H., Ree, J.-H., 2006. Weakening of deforming granitic rocks with layer development at middle crust. J. Struct. Geol. 28, 919–928.
Passchier, C.W., Trouw, R.A.J., 2005. Microtectonics. Springer, Berlin Heidelberg, pp. 67–109.
Pennacchioni, G., Menegon, L., Leiss, B., Nestola, F., Bromiley, G., 2010. Development of crystallographic preferred orientation and microstructure during plastic deformation of natural coarse-grained quartz veins. J. Geophys. Res. B Solid Earth 115.
Peternell, M., Hasalová, P., Wilson, C.J.L., Piazolo, S., Schulmann, K., 2010. Evaluating quartz crystallographic preferred orientations and the role of deformation partitioning using EBSD and fabric analyser techniques. J. Struct. Geol. 32, 803–817.
Platt, J.P., Behr, W.M., 2011. Lithospheric shear zones as constant stress experiments. Geology 39, 127–130.
Poirier, J.P., 1980. Shear localization and shear instability in materials in the ductile field. J. Struct. Geol. 2, 135–142.
Regenauer-Lieb, K., Weinberg, R.F., Rosenbaum, G., 2006. The effect of energy feedbacks on continental strength. Nature 442, 67–70.
Regenauer-Lieb, K., Yuen, D.A., 2006. Quartz rheology and short-time-scale crustal instabilities. Pure Appl. Geophys. 163, 1915–1932.
Rennie, S.F., Fagereng, Å., Diener, J.F.A., 2013. Strain distribution within a km-scale, mid-crustal shear zone: the Kuckaus Mylonite Zone, Namibia. J. Struct. Geol. 56, 57–69.
Rutter, E.H., Brodie, K.H., 2004. Experimental grain size-sensitive flow of hot-pressed Brazilian quartz aggregates. J. Struct. Geol. 26, 2011–2023.
Scheidegger, A.E., 1965. On the statistics of the orientation of bedding planes, grain axes, and similar sedimentological data. In: U.S. Geologic Survey.
Schmid, S.M., Casey, M., 1986. Complete Fabric Analysis of Some Commonly Observed Quartz C-axis Patterns, Mineral and Rock Deformation: Laboratory Studies. AGU, Washington, DC, pp. 263–286.
Schmid, S.M., Handy, M.R., 1991. Towards a Genetic Classification of Fault Rocks: Geological Usage and Tectonophysical Implications. Academic Press, London.
Shea, W.T., Kronenberg, A.K., 1993. Strength and anisotropy of foliated rocks with varied mica contents. J. Struct. Geol. 15, 1097–1121.
Song, W.J., Ree, J.H., 2007. Effect of mica on the grain size of dynamically recrystallized quartz in a quartz-muscovite mylonite. J. Struct. Geol. 29, 1872–1881.
Stipp, M., Stünitz, H., Heilbronner, R., Schmid, S.M., 2002. The eastern Tonale fault zone: a 'natural laboratory' for crystal plastic deformation of quartz over a temperature range from 250 to 700 °C. J. Struct. Geol. 24, 1861–1884.
Stipp, M., Tullis, J., 2003. The recrystallized grain size piezometer for quartz. Geophys. Res. Lett. 30, 3–5. SDE 3-1-SDE.
Tullis, J., Wenk, H.R., 1994. Effect of muscovite on the strength and lattice preferred orientations of experimentally deformed quartz aggregates. Mater. Sci. Eng. A 175, 209–220.
Tullis, J., Yund, R.A., 1985. Dynamic recrystallization of feldspar; a mechanism for ductile shear zone formation. Geol. (Boulder) 13, 238–241.
Tullis, J., Yund, R.A., 1987. Transition from cataclastic flow to dislocation creep of feldspar: mechanisms and microstructures. Geology 15, 606–609.
Twiss, R.J., 1977. Theory and applicability of a recrystallized grain size paleopiezometer. Pure Appl. Geophys. Pageoph 115, 227–244.
Vollmer, F.W., 1990. An application of eigenvalue methods to structural domain analysis. Geol. Soc. Am. Bull. 102, 786–791.
Vollmer, F.W., 1995. C program for automatic contouring of spherical orientation data using a modified Kamb method. Comput. Geosciences 21, 31–49.
Wenk, H.R., Christie, J.M., 1991. Comments on the interpretation of deformation textures in rocks. J. Struct. Geol. 13, 1091–1110.
White, S., 1976. The effects of strain on the microstructures, fabrics, and deformation mechanisms in quartzites. Philosophical Trans. R. Soc. Lond. Ser. A, Math.

Phys. Sci. 283, 69–86.
Wilson, C.J.L., 1979. Boundary structures and grain shape in deformed multilayered polycrystalline ice. Tectonophysics 57, T19–T25.
Wilson, C.J.L., Russell-Head, D.S., Kunze, K., Viola, G., 2007. The analysis of quartz c-axis fabrics using a modified optical microscope. J. Microsc. 227, 30–41.
Wightman, R.H., Prior, D.J., Little, T.A., 2006. Quartz veins deformed by diffusion creep-accommodated grain boundary sliding during a transient, high strain-rate event in the Southern Alps, New Zealand. J. Struct. Geol. 28, 902–918.
Woodcock, N.H., 1977. Specification of fabric shapes using an eigenvalue method. Geol. Soc. Am. Bull. 88, 1231–1236.
Yund, R.A., Tullis, J., 1984. Grain size reduction weakening of feldspars due to dynamic recrystallization. Eos, Trans. Am. Geophys. Union 65, 279.
Zhanga, X., Harkness, R.M., Last, N.C., 1992. Evaluation of connectivity characteristics of naturally jointed rock masses. Eng. Geol. 33, 11–30.